PNAS RESEARCH ARTICLE | EARTH, ATMOSPHERIC, AND PLANETARY SCIENCES

Planetary chaos and inverted climate phasing in the Late Triassic of Greenland

Malte Mau[a], Dennis V. Kent[b,c,1], and Lars B. Clemmensen[a,1]

Edited by Jean Jouzel, Laboratoire des Sciences du Climat et de L'Environ, Orme des Merisiers, France; received October 13, 2021; accepted March 12, 2022

Sedimentological records provide the only accessible archive for unraveling Earth's orbital variations in the remote geological past. These variations modulate Earth's climate system and provide essential constraints on gravitational parameters used in solar system modeling. However, geologic documentation of midlatitude response to orbital climate forcing remains poorly resolved compared to that of the low-latitude tropics, especially before 50 Mya, the limit of reliable extrapolation from the present. Here, we compare the climate response to orbital variations in a Late Triassic midlatitude temperate setting in Jameson Land, East Greenland (∼43°N paleolatitude) and the tropical low paleolatitude setting of the Newark Basin, with independent time horizons provided by common magnetostratigraphic boundaries whose timing has been corroborated by uranium-lead (U-Pb) zircon dating in correlative strata on the Colorado Plateau. An integrated cyclostratigraphic and magnetostratigraphic age model revealed long-term climate cycles with periods of 850,000 and 1,700,000 y ascribed to the Mars–Earth grand orbital cycles. This indicates a 2:1 resonance between modulation of orbital obliquity and eccentricity variations more than 200 Mya and whose periodicities are inconsistent with astronomical solutions and indicate chaotic diffusion of the solar system. Our findings also demonstrate antiphasing in climate response between low and midlatitudes that has implications for precise global correlation of geological records.

cyclostratigraphy | Milankovitch | lacustrine | Fleming Fjord Group

Significance

Our study of climate response to orbital variations in a Late Triassic midlatitude temperate setting in Jameson Land, East Greenland, provides robust evidence of astronomically forced grand cycles ascribed to gravitational interactions between Earth and Mars and is an Early Mesozoic record where both Mars–Earth modulation components are present and constrained with adequate chronostratigraphic controls. These findings suggest chaotic behavior of the inner Solar System and have implications as reference points in calculations of the past motions of the planets in the Solar System. Furthermore, our findings demonstrate a climate antiphasing between low and midlatitudes, which has implications for precise correlation of geological records and for validating models of Earth's climate dynamics.

Modern astronomical solutions provide powerful tools for constructing high-precision geologic age models by tuning a cyclostratigraphic response to theoretical variations in insolation for eccentricity, obliquity, and precession (1). This has been demonstrated by cyclostratigraphic studies of the Cenozoic era revealing the presence of a marine-integrated response to astronomical cycles predicted by modern astronomical solutions (2). However, cyclostratigraphic records from geological ages beyond ∼50 Mya cannot be calibrated to present astronomical solutions due to uncertainties created by numerical integration error and suspected chaotic behavior of the solar system (3). These uncertainties are especially reflected in the period of the two orbital grand cycles produced by the motions of Earth and Mars, the obliquity ($s_4 - s_3$) and eccentricity ($g_4 - g_3$) grand cycles (3), with present-day periods of 1.25 My and 2.45 My, respectively (4). During the last 30 My, Mars–Earth grand cycles have been in 2:1 secular resonance (3, 5). However, at some point in time prior to 50 Mya, modeling indicates that the inner planets of the Solar System experienced significant chaotic diffusion. This could result in a transformation of the 2:1 Mars–Earth resonance into either a new 1:1 resonance state or the same 2:1 resonance but with different periodicities (3, 6, 7). Geological evidence of these Mars–Earth cycles as long-term modulations of eccentricity and obliquity cycles is essential information to discriminate between various orbital solutions and to significantly improve the validity of these beyond ∼50 Mya. This could pave the way for more precise geologic time scales, provide a better understanding of climate events that are thought to be forced by these long-term cycles (8–10), constrain the existence of additional past planets, and provide further tests of gravitational models (11).

The Jameson Land Basin in central East Greenland contains a well-exposed Late Triassic lacustrine succession in the Fleming Fjord Group that was situated at a ∼43°N paleolatitude during Late Triassic times (Fig. 1*A*) (12, 13). The sediments contain a rich vertebrate fauna (14–20), which has been placed within a magnetostratigraphic context for global correlations and dating (13, 21). These lake deposits provide an orbitally paced midlatitude climate record, which enables the detection of eccentricity modulated precession as well as obliquity-paced signals. This permits the cyclostratigraphic record to uncover the full distribution of orbital cycles, including long-term

Author affiliations: [a]Department of Geosciences and Natural Resource Management, University of Copenhagen, Copenhagen K DK-1350, Denmark; [b]Lamont–Doherty Earth Observatory, Columbia University, Palisades, NY 10968; and [c]Earth and Planetary Sciences, Rutgers University, Piscataway, NJ 08854

Author contributions: M.M. and L.B.C. designed research; M.M., D.V.K., and L.B.C. performed research; M.M. and D.V.K. analyzed data; and M.M., D.V.K., and L.B.C. wrote the paper.

The authors declare no competing interest.

This article is a PNAS Direct Submission.

[1]To whom correspondence may be addressed. Email: dvk@ldeo.columbia.edu or larsc@ign.ku.dk.

This article contains supporting information online at http://www.pnas.org/lookup/suppl/doi:10.1073/pnas.2118696119/-/DCSupplemental.

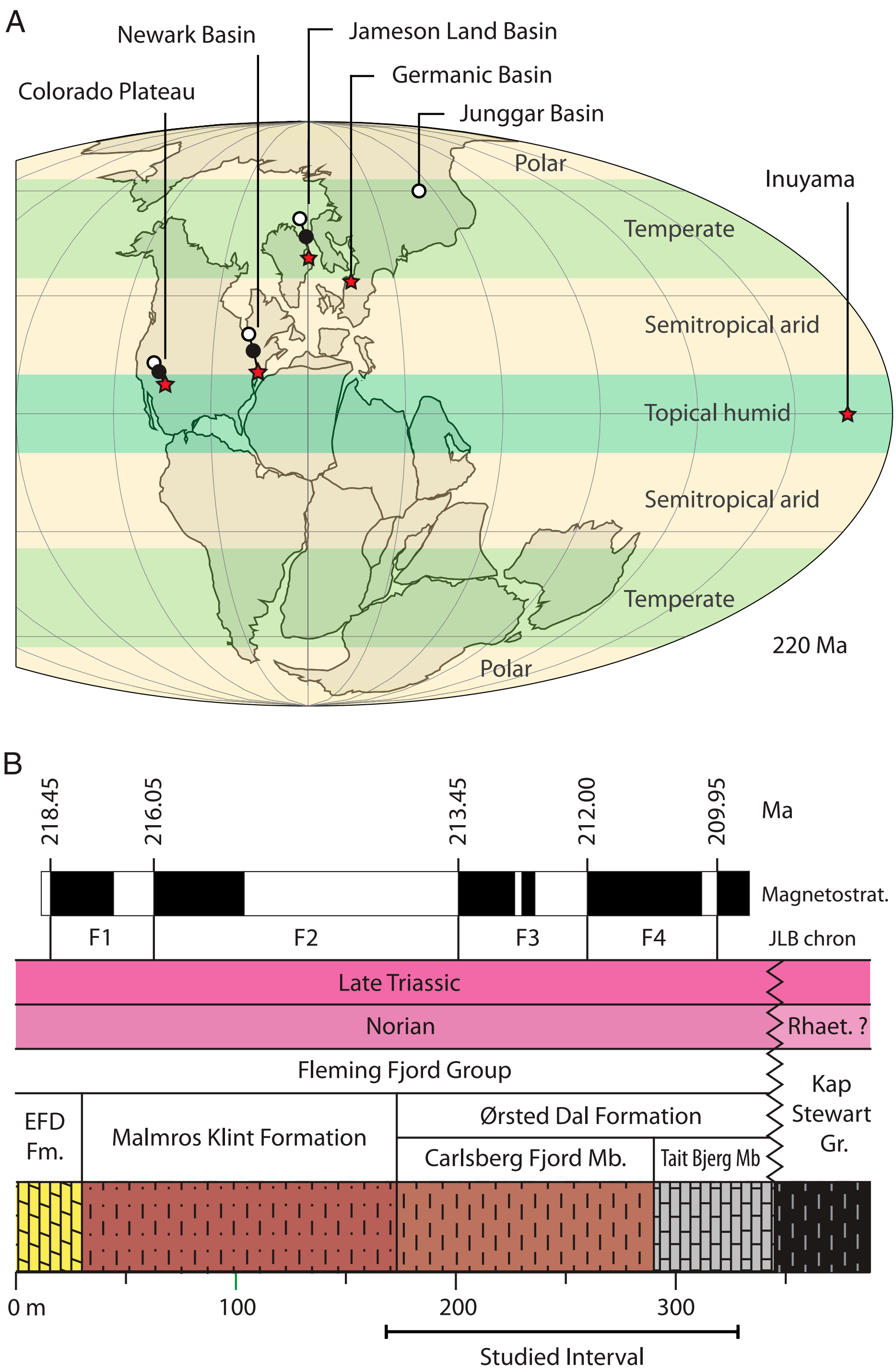

Fig. 1. Geologic setting of the Jameson Land Basin and some other Late Triassic basins mentioned in the text. (*A*) Paleogeographic reconstruction for 220 Mya of the Late Triassic (23) illustrating locations of the sedimentary basins mentioned in the text, where red stars are positions for 220 Mya, closed circles are positions for 210 Mya, and open circles are positions for 200 Mya. Generalized climate belts are from ref. 44. (*B*) Simplified stratigraphic log with magnetozones F1, F2, F3, and F4 from the Jameson Land Basin (JLB) (13) correlated to magnetochrons E13, E14, E15, and E16, respectively, from the N-H APTS that also provides the numerical age framework (23). The studied interval is indicated. EFD Fm, Edderfugledal Formation; JLB, Jameson Land Basin; Rhaet, Rhaetian; Magnetostrat, Magnetostratigraphy.

modulations of obliquity cycles, which are typically very weak in low-latitude tropical basins. The combination of magnetostratigraphy and cyclostratigraphy provides a powerful way to construct a high-precision age model for these ancient climate cycles whereby the geomagnetic polarity sequence has been calibrated with the stable long eccentricity (405 ky) metronome (22, 23). The resulting integrated age model allows for a precise record of the response to orbital variations in a midlatitude temperate climate setting of the Jameson Land Basin that can be compared to the low-latitude setting of the Newark Basin linked with time horizons provided by common magnetostratigraphic boundaries. This study analyzes a 165-m–thick red bed succession in the upper part of the Fleming Fjord Group comprising the Carlsberg Fjord Member and lower half of the overlying Tait Bjerg Member of the Ørsted Dal Formation. The magnetostratigraphic correlation of this part of the Fleming

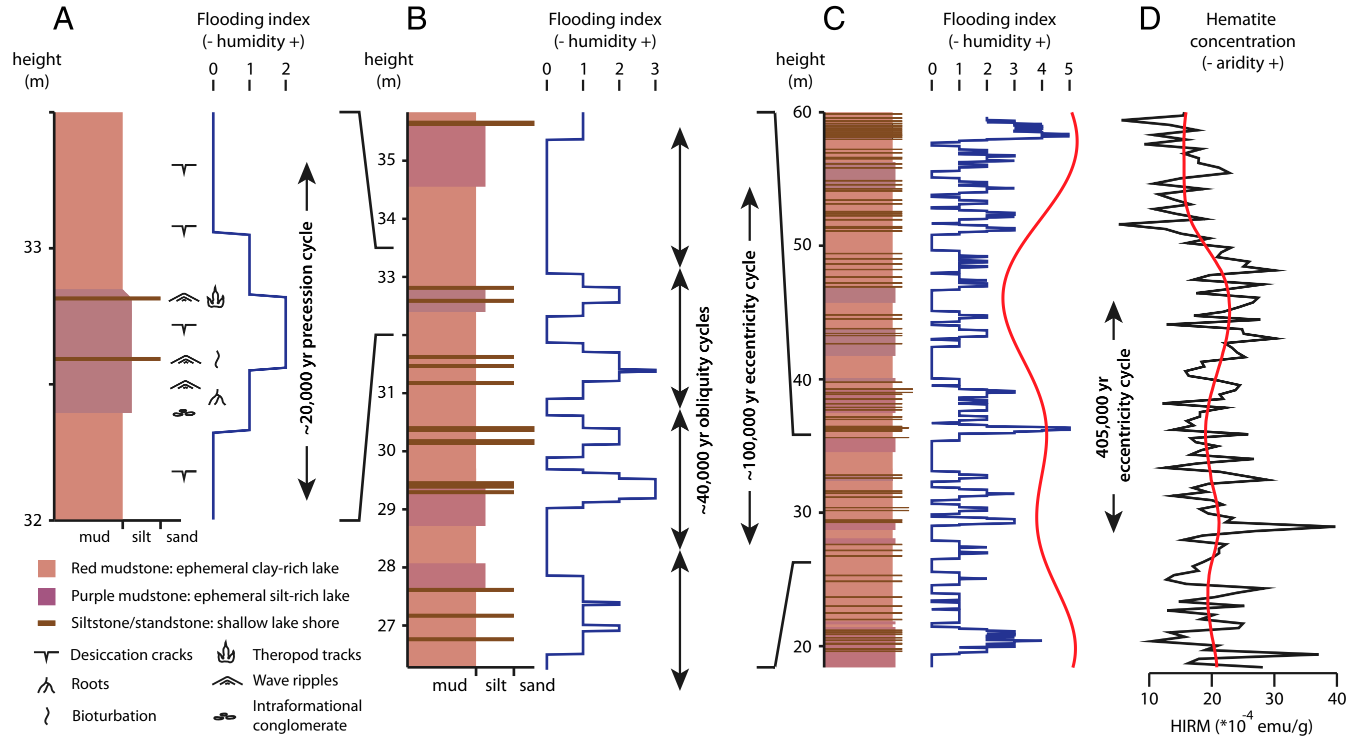

Fig. 2. Representative lithological cycles in the red bed secession of the Fleming Fjord Group based on field data from the lower part of the Carlsberg Fjord Member. (*A*) Basic meter-scale precessional cycle with typical sedimentary structures. (*B*) Obliquity cycles appear as alternating modifications of the precessional cycle. The short eccentricity cycle (100 ky) is expressed as bundling and amplitude modulation of around five basic precessional cycles. (*C*) The long eccentricity cycle (405 ky) expressed as bundling and amplitude modulation of basic precessional cycles. (*D*) Fluctuations in hematite concentration show higher aridity coinciding with a low FI and vice versa. Red lines are filtered signals (bandpass). Hard IRM fraction (HIRM) in c.g.s. electromagnetic units per gram. The FI is based on a simple moving average over a 0.5-m depth interval.

Fjord Group has been updated (13) to magnetochrons E14r to E17n of the Newark–Hartford astrochronostratigraphic polarity time scale (N-H APTS [23]), spanning an age of ∼214 to 210 Mya in the Norian.

Results

Climate and Cyclostratigraphy. A quasicyclic bedding has long been evident in exposures of the Fleming Fjord Group by color variation and the erosional profile (e.g., ref. 18). In the section of the Ørsted Dal Formation studied here, this variation is created by alternating red and purple mudstones, which are punctuated by centimeter-scale red to gray siltstone and sandstone beds. These red beds, corresponding to the Carlsberg Fjord Member, were deposited in a muddy ephemeral lake system (Fig. 1*B*). In the upper part of the studied succession corresponding to the Tait Bjerg Member, the sediments alternate between red beds and gray marlstone and limestone beds, interpreted as a more perennial lake system (12, 18). The mudstones are likely deposited from suspended material carried into the basin from the adjacent upland areas, with a possible minor input of wind-blown dust, including reworked soil aggregates (18, 24). The red mudstones are generally structureless but do contain desiccation cracks, whereas the purple mudstones are more coarse grained than the red mudstones and show occasional lamination, wave ripple marks, and plant roots (Fig. 2). Thus, the purple mudstones indicate periods with more humid climate and transport of more coarse-grained material to the basin. However, the mudstones represent a very ephemeral lacustrine environment with dominating mudflat deposition. Only during periods of increased precipitation did the water level in the basin increase sufficiently to allow short-lived transgressions of the former dry mudflat and deposition of thin (<10 cm) wave-rippled siltstones and occasional sandstones reworked by wind-driven waves and deposited across the basin (25). The alternation between siltstones and mudstones is the greatest source of lithological variation in the Ørsted Dal Formation. The occurrence of siltstone and sandstone beds displays a cyclic bundling in the form of spacing/frequency and bed thicknesses (Fig. 2). Thus, a higher frequency of siltstone and sandstone beds represents periods with more frequent humid climate and lake highstand. This is quantified by generating a flooding index (FI) that represents the frequency of siltstone beds calculated as a simple moving average over a specific distance or time interval (*Materials and Methods*). The use of the FI as a lithological humidity proxy is supported by hematite fluctuations used as an aridity proxy (Fig. 2) and additional climate proxies (SI Dataset).

The lithological series reveal cyclic climate variations of the sedimentary and environmental characteristics of the lake system that are similar to the very shallow lake setting in the contemporaneous part of the Newark Basin section (26). In the case of the Fleming Fjord cyclicity, shown diagrammatically for the lower part of the studied section in Fig. 2, the basic meter-scale lithological cycles are interpreted as combinations of precessional and obliquity cycles of Earth's rotation axis, where the precessional cycles tend to be bundled in what can be interpreted as modulation by ∼100-ky orbital eccentricity cycles and further in a ∼18-m cycle corresponding to the 405-ky–long eccentricity modulation cycle. This interpretation is supported by statistical analysis of several climate proxies (SI Dataset). A comparable pattern of nested lithologic cycles containing similar orbital period ratios is also recognized in Norian playa deposits in the Germanic Basin (27) (Fig. 1*A*). However, the precession and obliquity cycles are poorly developed in the

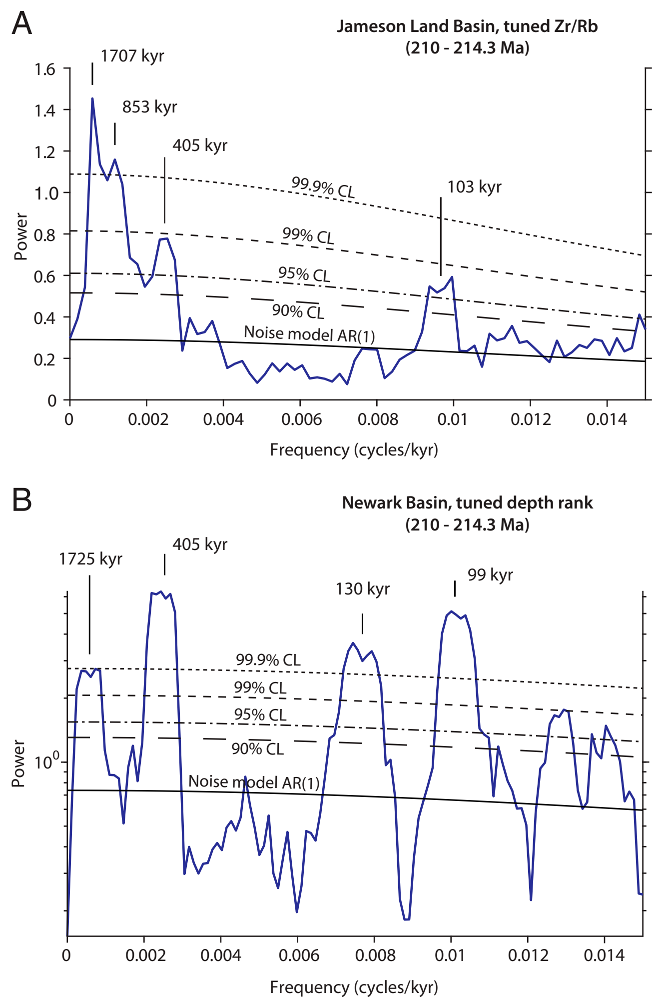

Fig. 3. Comparison of Thompson MTM analyses of the age-equivalent Jameson Land Basin and the Newark Basin climate records. (*A*) MTM spectrum of the zirconium/rubidium (Zr/Rb) record tuned to magnetostratigraphic chrons and the 405-ky metronome. The power spectrum from the Jameson Land Basin section shows a 103-ky cycle and a 405-ky cycle (approximation of 405 ky used in correlative N-H APTS) corresponding to short and long eccentricity. Furthermore, an 853-ky cycle and a 1,707-ky cycle corresponding to the two Mars–Earth grand cycles ($s_4 - s_3$ and $g_4 - g_3$, respectively) are present. (*B*) The power spectrum from the age equivalent but higher resolution record of depth rank from Newark Basin section (11) shows a 99-ky cycle and a 130.3-ky cycle corresponding to short eccentricity. The 405-ky peak corresponds to the long eccentricity cycle (which was used for tuning the section), while the 1,725-ky cycle corresponds to the eccentricity modulating Mars–Earth cycle ($g_4 - g_3$). CL, confidence level; AR, autoregressive.

Jameson Land Basin record, smeared and shifted to somewhat lower frequencies than predicted by astronomical solutions. This is most likely due to accumulation rate variability and a limited sampling rate in a relatively low-resolution record overall (SI Dataset) but not uncommonly found in statistical analyses of ancient lacustrine deposits (26, 28). Even in the thick lacustrine deposits of the Eocene Green River Formation, which could be considered a more recent analog of the Jameson Land Basin situated in a similar temperate belt setting in a high greenhouse world (29, 30), obliquity cyclicity has a weak lithologic expression (31) even though its contribution has been confirmed by formal multitaper method (MTM) spectral analysis (32).

Long-Term Climate Cycles. More clearly expressed in statistical tests and filtering of the Jameson Land Basin record are two long-term cycles with periods of 853 ky and 1,707 ky with respect to the interpreted 405-ky peak in the power spectral density (PSD) plot (Fig. 3) and that are readily filtered from the FI record (Fig. 4). The 1,707-ky cycle closely matches a long-term cycle of similar periodicity (∼1,725 ky) found in the Late Triassic record of the Newark Basin and most probably corresponds to the Mars–Earth eccentricity grand cycle ($g_4 - g_3$) (11). In fact, this ∼1,700-ky cycle is noticeably expressed as a long-term amplitude and frequency modulation of the 405-ky signal in both geochemical and lithological records in the Jameson Land Basin, as expected for the $g_4 - g_3$ term (3). The obliquity grand cycle ($s_4 - s_3$) has yet to be convincingly corroborated in the contemporaneous low-paleolatitude Newark record but might be expected in the higher-latitude Jameson Land Basin record, which contains a discernable obliquity signal. Indeed, comparison between spectral analyses of the 210.0- to 214.3-My interval corresponding to the studied succession reveals that no significant signal is present at a ∼850-ky period in between the much weaker 923-ky and 720-ky eccentricity cycles identified in the Newark Basin (11), even though both the Jameson Land record and corresponding interval of the Newark record a prominent ∼1,700-ky cycle (Fig. 3). Furthermore, comparisons of filtered ∼40-ky obliquity cycles and ∼850-ky cycles in the Jameson Land Basin indicate that the obliquity cycle is amplitude modulated by the ∼850-ky cycle (SI Dataset). We are thus confident in interpreting the 850-ky cycle found in the Jameson Land Basin as reflecting the obliquity modulating grand cycle ($s_4 - s_3$).

Mid- Versus Low-Latitude Orbital Phases. Magnetostratigraphic anchoring of the orbitally paced climate cycles in the Jameson Land Basin enables a comparison of relative phase and amplitude relationships with forcing from known 405-ky eccentricity modulation in the Newark Basin. The Jameson Land Basin record is converted from depth domain to time domain by tuning the depth record to the 405-ky metronome and magnetostratigraphic boundaries correlated with the Newark Basin (SI Dataset). Correlation of the tuned FI with the Newark Basin depth rank reveals that the humid peaks of the 405-ky–long eccentricity cycle ($g_2 - g_5$) as well as the ∼1,700-ky grand eccentricity cycle ($g_4 - g_3$) are about 180° out of phase between the basins (Fig. 4). In the Jameson Land Basin, intervals with a high frequency of major lake flooding (higher FI), coarser grain sizes (higher Zr/Rb), and less hematite (lower hard isothermal remanent magnetization [HIRM]) correlate with a low depth rank (i.e., lake low stand) in the Newark Basin. Thus, when the Jameson Land Basin was in a humid climate phase, the Newark Basin was in an arid climate phase and vice versa. The antiphasing between the basins is clearly seen at common magnetostratigraphic boundaries. For example, an FI peak (humid climate peak) at magnetic polarity boundary between magnetozones F2r and F3n in the midlatitude Jameson Land Basin corresponds to a low in-lake depth index (more arid climate) at correlative chron boundary E14r/E15n in the low-latitude Newark Basin (Fig. 4). In the same way, FI troughs at magnetic polarity boundaries F3n/F3r and F3r/F4n at midlatitude Jameson Land correspond to lake level peaks at correlative chron boundaries E15n/E15r and E15r/E16n at low-latitude Newark. These magnetostratigraphic boundaries are considered globally synchronous time horizons (33) and provide a unique framework for spatiotemporal mapping of climate cycles.

Discussion

Implications for Earth and Solar System Modeling. Grand cycles longer than 405 ky have been recognized in several Late

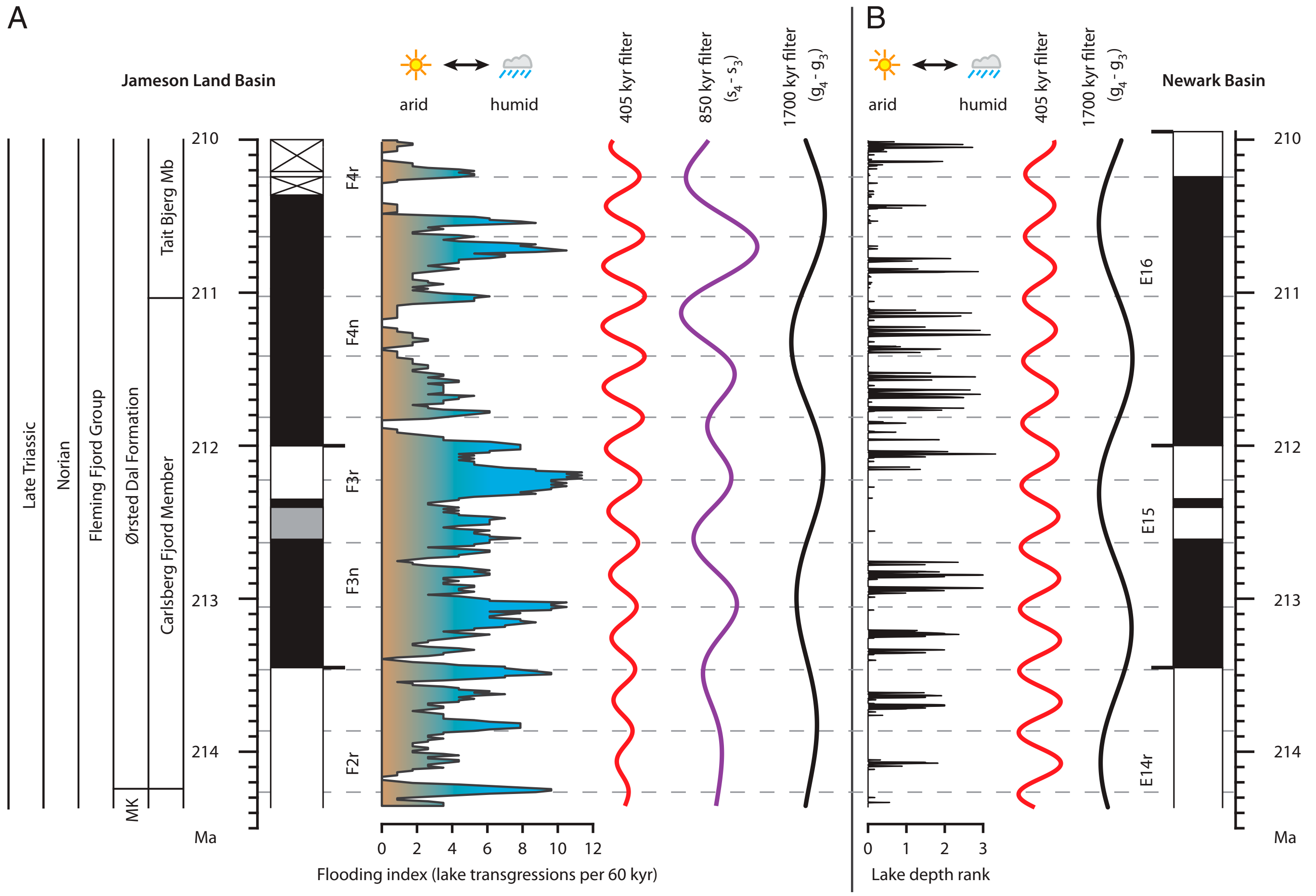

Fig. 4. Comparison of the timing of filtered low-frequency cycles in contemporaneous intervals from the Jameson Land Basin and the Newark Basin. (*A*) Data from the Jameson Land Basin (this study). (*B*) Data from the Newark Basin (11). The red filters represent the 405-ky cycle and are constructed with a bandpass filter range of 360 to 440 ky. The purple filter represents the 850-ky cycle and is constructed with a bandpass filter range of 700 to 1,200 ky. The black filters represent the ~1,700-ky cycle and are constructed with a bandpass filter range of 1, 400 to 2,000 ky. The FI is based on a simple moving average over a 60-ky time interval. Crossed areas in the polarity record mark intervals with poor data, while the gray area marks an interval with poor paleomagnetic data and possible missing evidence for a reversed polarity chron. This reversed chron is exposed in other magnetostratigraphic records of the Fleming Fjord Group (13) and represents a very short depth interval.

Triassic successions. A 1,725-ky eccentricity modulating grand cycle was found in the Newark Basin (11), and virtually the same cycle (with a reported period of 1,800 ky) was identified in marine cherts in the Inuyama area in present-day Japan (34). This suggests a shift of the modern 2,450-ky cycle (4) to a period of 1,700 to 1,800 ky in the Late Triassic. However, the obliquity modulating grand cycle has not been observed in either the Newark Basin or the Inuyama area most probably due to their low latitude depositional environments where insolation changes from obliquity forcing are expected to be minimal. A hint of a long (~820-ky) obliquity modulating grand cycle was reported in a study of the high-latitude Late Triassic–Early Jurassic Junggar Basin section (27), although the record was characterized (11) as lacking an independent geochronology or paleomagnetic polarity record for correlation. Thus, none of the previous Late Triassic studies have been able to adequately constrain the obliquity modulating grand cycle for comparison to the eccentricity grand cycle in the same or time-correlative record, which is, in theory, possible in mid- to high-latitude records (3, 35).

The shift of the $g_4 - g_3$ component from the present-day 2,450-ky period to a ~1,700-ky period and the concomitant shift of the $s_4 - s_3$ component from the present-day 1,250-ky period to an ~850-ky period are inconsistent with astronomical solutions and provide direct evidence of the chaotic behavior of the inner planets of the solar system. The periods found in this study result in a 2:1 Mars–Earth resonance state, which is identical to the present-day 2:1 ratio of eccentricity to inclination. Thus, although some solar system modeling suggests a transition to the modern 2:1 ratio from a 1:1 resonance state sometime before the limit of computational extrapolation at 50 Mya and a Cretaceous (~90 Mya) sequence that offers tantalizing evidence of a 1:1 resonance state (36), our evidence from the ~214- to 210-Mya record in the Jameson Land Basin shows that a 2:1 resonance state prevailed in the Late Triassic and implies that one or more additional transitions in resonance state occurred in the intervening time interval. The results from our study provide a constraint for Solar System chaos and Mars–Earth secular resonance for ~214.4 to 210 Mya, which can be used as a reference point in future astronomical solutions for the Late Triassic.

An unexpected finding in our study is the inverted climate response to eccentricity cycles in the midlatitude Jameson Land Basin compared to the low-latitude Newark Basin whereby the filtered ~1,700-ky cycle is remarkably anticorrelated with the filtered ~1,700-ky cycle in the Newark Basin, just like the climate response to the 405-ky cycle that anticorrelates between the basins (Fig. 4). The phase parallelism of the 405-ky metronome and the ∼1,700-ky grand cycle supports their correct identification. Recognizing that the Jameson Land Basin record is from the temperate humid belt whereas the correlative portion of the Newark Basin record is ∼30° closer to the equator from the semitropical arid belt (Fig. 1*A*), we can attempt to explain the latitudinal inversion of eccentricity insolation forcing by analogy with latitudinal differences in climate response to changing atmospheric CO_2 concentration in general circulation models (37). As atmospheric CO_2 concentration increases, such modeling experiments show a decrease in net moisture or runoff (i.e., reduced precipitation minus evaporation [P – E]) in the semitropical arid belt but an increase in P − E in the bounding temperate and equatorial humid belts related to intensification of the Hadley cell. Pending testing with global climate modeling, we suggest that the latitudinal pattern of change in P − E with greenhouse climate forcing may be similar to change in insolation forcing from eccentricity whereby the climate response (P − E) will be opposite in the semitropical arid belt (Newark Basin) and temperate humid belt (Jameson Land Basin), as indicated by the empirical data. General circulation models also show that obliquity-driven insolation creates increased poleward moisture transport in temperate latitudes during Northern Hemisphere summer at low tilt angles (38, 39). Although not expected to influence correlation of the temperate latitude Jameson Land Basin record with the subtropical Newark Basin record, which does not have an obliquity signal, climate antiphasing from obliquity forcing could potentially be produced with respect to lacustrine and fluvial records from polar latitudes, such as the Junggar Basin. We conclude that climate belts are an important consideration when correlating cyclostratigraphic records across latitudes, as they might show inverted climate phase response, which if not realized could produce significant temporal offsets (e.g., ∼200 ky in the case of the 405-ky eccentricity cycle). This could have important implications for detailed age control based on correlation using cyclostratigraphy and the astrochronostratigraphic polarity time scale (23).

All lithostratigraphic subunits in the Fleming Fjord Group display a quasicyclic bedding that is most probably orbitally forced (18). Thus, the 160-m cyclostratigraphic record presented in this study has the potential to be eventually extended to a 300- to 400-m–thick succession that represents the entire Fleming Fjord Group and a time span of about 11 My (13). Such an extended record would provide more secure context for analysis of long-term climate cycles (11) and could further validate the Mars–Earth orbital cycles we already see imprinted in the upper part of the Fleming Fjord Group. Several localities along the western shore of the Carlsberg Fjord have optimal exposure conditions for field studies of most of the Fleming Fjord Group. In particular, Tait Bjerg would be a well-suited study site since paleomagnetic data have already been published in the Carlsberg Fjord Member and the Malmros Klint Formation at this locality (13). Another desired improvement would be more closely spaced measurements of lithofacies and elemental compositions, which could be done at selected sites with continuous, clean, and well-exposed cliff or ravine sections in the Edderfugledal and Malmros Klint Formations; this would allow better resolution of short-period precession and obliquity cycles now obscured by relatively coarse sampling intervals. Ultimately, a continental scientific coring project targeting complete recovery of the Fleming Fjord Group would be the most optimal method for enhancing this unique temperate latitude cyclic record for the Late Triassic.

Materials and Methods

Rock Sample Analyses. Each locality was sampled for cyclostratigraphic analysis every 33 to 35 cm, resulting in a Nyquist wavelength of ∼70 cm. Samples for paleomagnetic analyses were collected every 1.75 m. All samples were collected from fresh sediments in pits dug centimeters to decimeters below the surface. Samples collected for cyclostratigraphic analysis were rinsed with demineralized water, dried at 50 °C, and crushed with a vibratory ball mill before analysis. X-ray flourescence (XRF) analyses were performed with a fixed Olympus Delta Premium DP-6000 XRF analyzer at the Department of Geosciences and Natural Resource Management XRF laboratory (University of Copenhagen). Each sample was analyzed for 2 × 120 s with a 10-kV beam and a 30-kV beam. The crushed samples were covered with thin Mylar film to improve the detection limit of the lightest elements. The accuracy was regularly tested by reanalyzing samples and by analyzing the marine sediment certified reference material PACS-3 and pure SiO_2. Color analyses were performed with a Voltcraft plus RGB-2000 color analysis device on crushed bulk samples through thin film. The measured 10-bit red-green-blue (RGB) values provide a resolution of 1,024 shades of each primary color. The RGB color space was converted to the International Commission on Illumination L*a*b* (CIELAB) color space with the rgb2lab function in Matlab. The entire Carlsberg Fjord Member was sampled for magnetostratigraphy in 2018. The same paleomagnetic field sampling, laboratory, and analytical procedures were followed as for the 1992 and 1995 sample sets as described previously (13, 21). This basically involved complete progressive thermal demagnetization in 12 or more steps to 680 °C to isolate components of natural remanent magnetization in the oriented samples. For remanent coercivity analysis, the isothermal remanent magnetization (IRM) of sample chips were measured after being subjected to a 1-T magnetic field pulse. The samples were then remeasured after exposure to a 300-mT backfield to gauge the contribution from lower coercivity magnetite and maghemite. The magnetically hard IRM fraction (HIRM) attributable to hematite was calculated with $0.5 \times (\mathrm{IRM}_{+1\ \mathrm{T}} + \mathrm{IRM}_{-300\ \mathrm{mT}})$. IRM were produced with an ASC Scientific model IM-10-30 impulse magnetizer; thermal demagnetizations were done in an ASC Scientific TD48 oven, and all sample remanences were measured in a 2G, Inc. model 760 3-axis DC SQUID magnetometer housed in a magnetically shielded room at the LDEO Paleomagnetics Laboratory.

Signal Processing. All PSD plots were estimated with the Thomson MTM (40) using the "pmtm" function from the signal processing toolbox in Matlab. The time–bandwidth product (NW) was set to 2. The number of tapers used to calculate the PSD was by default 2 × NW – 1, resulting in three tapers. The fast Fourier transform was set to the next power of 2 greater than the length of the dataset. To remove unwanted effects caused by other factors than orbital cycles, the datasets were detrended before the MTM analysis by removing the best linear fit. MTM confidence levels were estimated with the robust autoregressive noise model AR1 (41). The evolutionary wavelet spectrum was computed with a Morlet wavelet with the Matlab script of ref. 42. Bandpass filters were constructed with the bandpass function from the signal processing toolbox in Matlab to extract cycles from the data. The Astronchron package in R (43) was used to tune the dataset to specified time points (the 405-ky metronome and magnetostratigraphic boundaries; SI Dataset) and interpolate the tuned stratigraphic series onto an evenly spaced data grid of one data point per 5 ky.

Construction of the FI. Climate-sensitive lithological data were quantified by generating a FI, which represents the frequency of siltstone beds throughout the lake succession. The FI was calculated as the simple moving average of the siltstone bed concentration over a specified depth or time interval. The moving average FI in Fig. 2 was created before tuning to the age model by adding all siltstone beds within a 0.5-m stratigraphic range to resolve the lithological cycles at decimeter scale. The moving average FI in Fig. 4 was created after tuning to the age model by adding all siltstone beds within a 60-ky time range to resolve the long-term lithological cycles.

Data Availability. All study data are included in the article and/or supporting information.

ACKNOWLEDGMENTS. We thank the Independent Research Fund Denmark for funding this project, the Geologic Survey of Denmark and Greenland for logistical help in the field, and the Paleomagnetic Research Fund at Lamont–Doherty Earth Observatory for the magnetostratigraphic work. We also thank Paul Olsen for helpful comments and suggestions to the manuscript, Jesper Milan for taking drone photos of the outcrops, Nicolai Frobøse for sampling and laboratory analyses of samples from the Tait Bjerg Member, and Christian Bjerrum for access to XRF equipment and for advice regarding sample collection for cyclostratigraphy. We would also like to thank two anonymous reviewers for constructive comments that helped us to improve the revised paper.

1. K. P. Kodama, L. A. Hinnov, *Rock Magnetic Cyclostratigraphy* (John Wiley & Sons, vol. 5, 2015)
2. T. Westerhold *et al.*, An astronomically dated record of Earth's climate and its predictability over the last 66 million years. *Science* **369**, 1383–1387 (2020).
3. J. Laskar, A. Fienga, M. Gastineau, H. Manche, La2010: A new orbital solution for the long-term motion of the Earth. *Astron. Astrophys.* **532**, A89 (2011).
4. L. A. Hinnov, New perspectives on orbitally forced stratigraphy. *Annu. Rev. Earth Planet. Sci.* **28**, 419–475 (2000).
5. H. Pälike, J. Laskar, N. J. Shackleton, Geologic constraints on the chaotic diffusion of the solar system. *Geology* **32**, 929–932 (2004).
6. J. Laskar, The chaotic motion of the solar system: A numerical estimate of the size of the chaotic zones. *Icarus* **88**, 266–291 (1990).
7. J. Laskar, "A few points on the stability of the Solar System" in *Symposium-International Astronomical Union* (Cambridge University Press, 1992), vol. 152, pp. 1–16.
8. L. J. Lourens *et al.*, Astronomical pacing of late Palaeocene to early Eocene global warming events. *Nature* **435**, 1083–1087 (2005).
9. H. Pälike *et al.*, The heartbeat of the Oligocene climate system. *Science* **314**, 1894–1898 (2006).
10. J. A. van Dam *et al.*, Long-period astronomical forcing of mammal turnover. *Nature* **443**, 687–691 (2006).
11. P. E. Olsen *et al.*, Mapping solar system chaos with the Geological Orrery. *Proc. Natl. Acad. Sci. U.S.A.* **116**, 10664–10673 (2019).
12. L. B. Clemmensen, D. V. Kent, M. Mau, O. Mateus, J. Milán, Triassic lithostratigraphy of the Jameson Land Basin (central east Greenland), with emphasis on the new Fleming Fjord Group. *Bull. Geol. Soc. Denmark* **68**, 95–132 (2020).
13. D. V. Kent, L. B. Clemmensen, Northward dispersal of dinosaurs from Gondwana to Greenland at the mid-Norian (215-212 Ma, Late Triassic) dip in atmospheric $p\mathrm{CO}_2$. *Proc. Natl. Acad. Sci. U.S.A.* **118**, e2020778118 (2021).
14. F. J. Jenkins *et al.*, Late Triassic continental vertebrates and depositional environments of the Fleming Fjord Formation, Jameson Land, east Greenland. *Medd. Gronl. Geosci.* **32**, 1–25 (1994).
15. M. Marzola, O. Mateus, J. Milan, L. B. Clemmensen, A review of Palaeozoic and Mesozoic tetrapods from Greenland. *Bull. Geol. Soc. Denmark* **66**, 21–46 (2018).
16. L. B. Clemmensen, Triassic rift sedimentation and palaeogeography of central East Greenland. *Bull. Grønlands geol. Unders.* **136**, 72 (1980).
17. L. B. Clemmensen, Triassic lithostratigraphy of East Greenland between Scoresby Sund and Kejser Franz Josephs Fjord. *Bull. Grønlands geol. Unders.* **139**, 56 (1980).
18. L. B. Clemmensen, D. V. Kent, F. A. Jenkins Jr., A Late Triassic lake system in East Greenland: Facies, depositional cycles and palaeoclimate. *Palaeogeogr. Palaeoclimatol. Palaeoecol.* **140**, 135–159 (1998).
19. L. B. Clemmensen *et al.*, The vertebrate-bearing Late Triassic Fleming Fjord Formation of central East Greenland revisited: Stratigraphy, palaeoclimate and new palaeontological data. *Geol. Soc. Lond. Spec. Publ.* **434**, 31–47 (2016).
20. T. Sulej *et al.*, The earliest-known mammaliaform fossil from Greenland sheds light on origin of mammals. *Proc. Natl. Acad. Sci. U.S.A.* **117**, 26861–26867 (2020).
21. D. V. Kent, L. B. Clemmensen, Paleomagnetism and cycle stratigraphy of the Triassic Fleming Fjord and Gipsdalen formations of East Greenland. *Bull. Geol. Soc. Denmark* **46**, 121–136 (1996).
22. D. V. Kent *et al.*, Empirical evidence for stability of the 405-kiloyear Jupiter-Venus eccentricity cycle over hundreds of millions of years. *Proc. Natl. Acad. Sci. U.S.A.* **115**, 6153–6158 (2018).
23. D. V. Kent, P. E. Olsen, G. Muttoni, Astrochronostratigraphic polarity time scale (APTS) for the Late Triassic and Early Jurassic from continental sediments and correlation with standard marine stages. *Earth Sci. Rev.* **166**, 153–180 (2017).
24. M. R. Talbot, K. Holm, , M. A. J. Williams, "Sedimentation in low-gradient desert margin systems: A comparison of the Late Triassic of northwest Somerset (England) and the late Quaternary of east-central Australia" in *Paleoclimate and Basin Evolution of Playa Systems*, M. R. Rosen, Eds. (Geological Society of America, vol. 289, 1994).
25. M. Mau, C. J. Bjerrum, L. B. Clemmensen, Late Triassic paleowinds from lacustrine wave ripple marks in the Fleming Fjord Group, central East Greenland. *Palaeogeogr. Palaeoclimatol. Palaeoecol.* **586**, 110776 (2022).
26. P. E. Olsen, D. V. Kent, Long-period Milankovitch cycles from the Late Triassic and Early Jurassic of eastern North America and their implications for the calibration of the Early Mesozoic time–scale and the long–term behaviour of the planets. *Philos. Trans. Royal Soc. A* **357**, 1761–1786 (1999).
27. T. Vollmer *et al.*, Orbital control on Upper Triassic Playa cycles of the Steinmergel-Keuper (Norian): A new concept for ancient playa cycles. *Palaeogeogr. Palaeoclimatol. Palaeoecol.* **267**, 1–16 (2008).
28. J. Sha *et al.*, Triassic–Jurassic climate in continental high-latitude Asia was dominated by obliquity-paced variations (Junggar Basin, Ürümqi, China). *Proc. Natl. Acad. Sci. U.S.A.* **112**, 3624–3629 (2015).
29. R. C. Surdam, C. A. Wolfbauer, Green River Formation, Wyoming: A playa-lake complex. *Geol. Soc. Am. Bull.* **86**, 335–345 (1975).
30. T. K. Lowenstein, R. V. Demicco, Elevated Eocene atmospheric CO_2 and its subsequent decline. *Science* **313**, 1928 (2006).
31. A. G. Fischer, L. T. Roberts, Cyclicity in the Green River formation (lacustrine Eocene) of Wyoming. *J. Sediment. Res.* **61**, 1146–1154 (1991).
32. S. R. Meyers, Resolving Milankovitchian controversies: The Triassic Latemar Limestone and the Eocene Green River Formation. *Geology* **36**, 319–322 (2008).
33. G. M. Muttoni, "Magnetostratigraphy" in *Encyclopedia of Geology*, D. Alderton, S. A. Elias, Eds. (Elsevier Ltd., ed. 2, 2021), pp. 689–697.
34. M. Ikeda, R. Tada, Reconstruction of the chaotic behavior of the solar system from geologic records. *Earth Planet. Sci. Lett.* **537**, 116168 (2020).
35. L. A. Hinnov, F. J. Hilgen, "Cyclostratigraphy and astrochronology" in *Cyclostratigraphy and Astrochronology. The Geologic Time Scale 2012*, F. M. Gradstein, J. G. Ogg, M. D. Schmitz, G. M. Ogg, Eds. (Elsevier, Amsterdam, vol. 1, 2012), pp. 63–83.
36. C. Ma, S. R. Meyers, B. B. Sageman, Theory of chaotic orbital variations confirmed by Cretaceous geological evidence. *Nature* **542**, 468–470 (2017).
37. S. Manabe, K. Bryan Jr., CO_2-induced change in a coupled ocean-atmosphere model and its paleoclimatic implications. *J. Geophys. Res. Oceans* **90**, 11689–11707 (1985).
38. D. F. Mantsis, A. C. Clement, A. J. Broccoli, M. P. Erb, Climate feedbacks in response to changes in obliquity. *J. Clim.* **24**, 2830–2845 (2011).
39. D. F. Mantsis *et al.*, The response of large-scale circulation to obliquity-induced changes in meridional heating gradients. *J. Clim.* **27**, 5504–5516 (2014).
40. D. J. Thomson, "Spectrum estimation and harmonic analysis" in *Proceedings of the IEEE* (IEEE, vol. 70, 1982) pp. 1055–1096.
41. M. Li, L. Hinnov, L. Kump, Acycle: Time-series analysis software for paleoclimate research and education. *Comput. Geosci.* **127**, 12–22 (2019).
42. C. Torrence, G. P. Compo, A practical guide to wavelet analysis. *Bull. Am. Meteorol. Soc.* **79**, 61–78 (1998).
43. S. R. Meyers, Astrochron: An R package for astrochronology (2014). https://cran.r-project.org/package=astrochron. Accessed 10 September 2019.
44. D. V. Kent, G. Muttoni, Latitudinal land–sea distributions and global surface albedo since the Cretaceous. *Palaeogeogr. Palaeoclimatol. Palaeoecol.* **585**, 110718 (2022).